ARGONNE NATIONAL LABORATORY
9700 South Cass Avenue
Argonne, Illinois 60439

ANL-01/29

ADVANCED SENSORS FOR REAL-TIME CONTROL OF COMBUSTION IN ADVANCED NATURAL-GAS RECIPROCATING ENGINES

by

S. H. Sheen, H. T. Chien, and A. C. Raptis

Energy Technology Division

October 2001

Work Sponsored by

U.S. DEPARTMENT OF ENERGY
Office of Power Technology

CONTENTS

FIGURES

TABLES

ACKNOWLEDGMENTS

This work was sponsored by the U.S. Department of Energy, Office of Power Technology.

ADVANCED SENSORS FOR REAL-TIME CONTROL OF COMBUSTION IN ADVANCED NATURAL-GAS RECIPROCATING ENGINES

by

S. H. Sheen, H. T. Chien, and A. C. Raptis

ABSTRACT

This report summarizes the first year effort and findings under a project to develop advanced sensors for real-time combustion monitoring of advanced natural-gas reciprocating engines. Two sensor technologies are described: an ion-mobility spectrometry (IMS) sensor to measure NO_x emissions and an acoustic sensor to determine natural-gas fuel composition. A spark-discharge ionization source is developed for the IMS sensor; its performance in detecting negative NO_x ions is presented. The acoustic sensor measures both speed of sound and attenuation in natural-gas mixtures. It is demonstrated that the acoustic relaxation due to vibrational degrees of freedom of methane can be measured. The baseline principles of each technology are outlined.

1.0 INTRODUCTION

This project, funded by Department of Energy, Office of Power Technology, was started in September 2000 and will be completed in September 2003. This report summarizes the first-year effort and findings. The baseline principles of each technology that the project proposes are described, and future work is outlined.

The objective of this project is to develop advanced sensors for real-time combustion monitoring of advanced natural-gas reciprocating engines. The proposed developments include sensors to measure NO_x emissions and fuel composition and a control system that optimizes engine performance and controls NO_x emissions.

To detect and monitor NO_x emissions in the range of 1-100 ppm, a nonradioactive ion-mobility spectrometry (IMS) sensor will be developed. The IMS sensor will detect negative NO_x ions in a high-pressure and -temperature environment. Another sensor that will be developed is based on a novel acoustic gas-sensor technology that determines fuel composition and flow rate by measuring the acoustic properties of the natural-gas flow. An integrated control system that will also be developed will use the IMS outputs to adjust the air/natural-gas ratio or fuel composition and thus optimize engine performance and control NO_x emissions.

2.0 PROJECT MANAGEMENT SUMMARY

Project Objectives: To develop advanced sensors and a control system for real-time control of combustion in advanced natural-gas reciprocating engines.

Major Tasks: (A) Development of an ion-mobility NO_x emission sensor
(B) Development of natural-gas fuel-composition sensor
(C) Development of real-time combustion-control system
(D) Field tests of sensors and control systems

Schedule:

Major Tasks	FY 2000	FY 2001				FY 2002				FY 2003			
	4Q	1Q	2Q	3Q	4Q	1Q	2Q	3Q	4Q	1Q	2Q	3Q	4Q
A	→	→	→	→	→								
B				→	→	→	→	→	→				
C									→				
D										→	→	→	→

Budget and Cost :

Total budget for FY2000-2001 ----------$ 550K

Total cost at end of FY2001 ----------$ 408.2K

3.0 DESCRIPTION OF SENSOR TECHNOLOGIES

In this section, we describe the basic design and operating principle of the two proposed gas sensors: IMS and acoustic natural gas.

3.1 Ion-Mobility Spectrometry Sensors

Figure 1 shows the basic design of an IMS sensor, which consists of an ion source, a drift tube, and an ion detector. The ion source ionizes gas molecules by either direct electron bombardment or ion-molecule reactions. Product ions are then extracted into the drift tube and move to the detector in a uniform electric field. The ion drift velocity, a measurable quantity with IMS, is influenced by the applied electrical field *E* and the ion concentration gradient *(∂n/∂x)* [1]. To include only the linear terms, the drift velocity is given by

$$V = KE - \frac{D}{n}\left(\frac{\partial n}{\partial x}\right), \tag{1}$$

where *n* is ion concentration; *D,* the diffusion coefficient; and *K,* the ion mobility. The diffusion term is generally very small, especially under ambient conditions. Thus, the ion drift velocity

provides a direct measure of ion mobility. Based on Eq. 1, the electric force may be balanced by the diffusion force needed to reach an equilibrium at which $V = 0$.

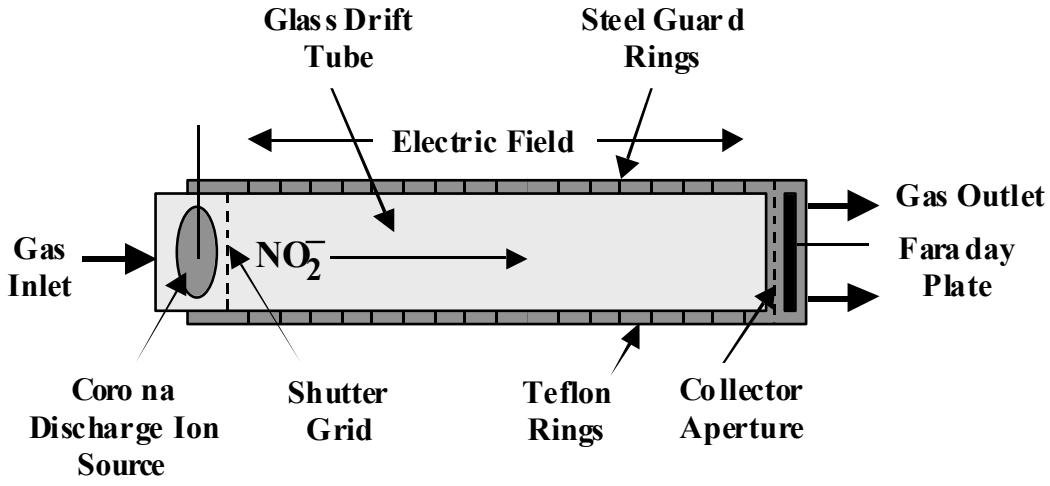

Fig. 1. Basic design of ion-mobility spectrometer

Assuming that the ion concentration follows a Boltzmann distribution, one can obtain the Nernst-Einstein relationship, which relates the ion mobility with the ion diffusion coefficient, given as

$$K = qD / kT, \tag{2}$$

where q is the charge and k, Boltzmann's constant. When the ion motion is not in equilibrium, the dominating effect is ion-neutral collisions, and the mobility is given by

$$K = \left(\frac{q}{n}\right)^{1/2}\left(\frac{1}{3\mu T_{eff}}\right)^{1/2}\left[\frac{1}{\Omega(T_{eff})}\right], \tag{3}$$

where μ is the reduced mass of ion and buffer gas, $T_{eff} = T + MV^2/3k$ (M is molecular weight of the buffer gas), and $\Omega(T_{eff})$ is the total scattering cross section. Conceptually, differing ions have differing mobilities in the same medium. But, just as mass spectrometry determines the charge/mass ratio, ion mobility determines the quantity of $(q/\mu)^{1/2}\Omega$. For heavy ions, μ is nearly equal to the mass of the neutral molecule (e.g., nitrogen), and Ω essentially measures the average cross-sectional area of the ion or the ion size. On the other hand, for a series of atomic ions in the same neutral gas, Ω is nearly constant, and the mobility is determined by the reduced mass, assuming that q is fixed. In practice, the buffer is a gas mixture. The mobility of an ion in a gas mixture can be approximated by Blanc's law [2], given as

$$\frac{1}{K} = \sum_j \frac{X_j}{K_j}, \tag{4}$$

where X_J is the mole fraction of the jth gas.

In principle, if all ion-molecule interactions that occur in the drift tube are known, the ion-mobility spectrum gives a fingerprint of the ions present. However, in practice, the peak position and shape depend on the gas-mixture composition, temperature, and flow rate. Therefore, each ion-mobility spectrometer may need a set of calibration data for its application in identifying ions. For quantitative measurement, the peak amplitude may be used.

In past work, Argonne National Laboratory developed a positive-ion-mode IMS sensor for detecting hydrocarbons [3]. Previous ANL work also demonstrated that good sensitivity in detecting NO_X can be obtained if the IMS sensor is operated in a negative-ion mode [4].

3.2 Acoustic Natural-Gas Sensors

The typical fuel of a natural-gas reciprocating engine [5] consists of 82-96% methane, 2-7% ethane, 0.4-1.1% propane, and up to 0.6% higher HCs. To optimize engine combustion we must monitor the fuel input to the engine, a task that requires real-time measurements of mass flow rate and gas composition. The developments proposed under this project include acoustic methods to measure flow rate, percent of natural gas in the flow, and gas composition. The first-year effort focused on acoustic techniques to measure natural-gas composition and concentration.

The acoustic method to measure the natural-gas concentration in a flow stream is based on measuring the sound speed. Under the assumptions that the gas under question behaves like an ideal gas and that the propagation of sound waves is an isentropic process, the speed of sound C_o can be given as

$$C_o = \left[\frac{RT}{\sum_{i=1}^{n} x_i M_i} \frac{\sum_{i=1}^{n} x_i C_{p_i}}{\sum_{i=1}^{n} \left(x_i C_{p_i} - R \right)} \right]^{1/2}, \tag{5}$$

where R is the gas constant; T, the absolute temperature; x_I, the mole fraction of gas I; M_I, molecular weight of gas I; and Cp_I, heat capacity of gas i under constant pressure. For binary gas mixtures, the mixture composition can be determined from speed-of–sound (SOS) measurements. For a multigas mixture, the same measurement may indicate the concentration change of a constituent in the mixture, especially, when the sound speed of the constituent is much different from that of other gases in the mixture, for example, helium in air [6]. The speeds of sound in major constituents [7] of a typical natural-gas mixture are listed in Table 1. Methane stands out from the other gases by at least 25%. Therefore, it is possible to monitor methane concentration by measuring the SOS in the natural-gas stream.

Table 1. Speed of sound (cm/s) in natural-gas constituents and air/carbon dioxide

Methane	Ethane	Propane	n-Butane	Air	Carbon Dioxide
446	316	253	216	346	270

Figure 2 shows the basic design of an SOS sensor that consists of two ultrasonic transducers coupled to a flow channel through which gas is pumped. The sensor operates in a pitch-catch mode and analyzes a higher order reflection so that better sensitivity can be obtained. Because the channel is narrow (0.5 in. in diameter), many reflections are detected. From these reflections, we can also deduce sound attenuation in the gas mixture.

To identify each constituent in a natural-gas mixture, we propose to measure attenuation as a function of ultrasonic frequency. Ultrasonic attenuation in a gas under isentropic conditions is primarily the result of effects due to viscosity drag and heat conduction. This is commonly referred to as classical attenuation α_{cl}, expressed (Eq. 6) in terms of a dimensionless μ_{cl} (= $\alpha_{cl}\lambda$, where λ is the wavelength) and frequency over pressure *f/P*:

$$\mu_{cl} = \frac{2\pi^2}{\gamma}\left[\frac{4}{3}\left(\eta + \frac{3}{4}\eta'\right) + \frac{\kappa(\gamma-1)}{C_P}\right]\frac{f}{P}. \tag{6}$$

In Eq. 6, C_P is the heat capacity at constant pressure of the gas, and η, η', γ, κ are, respectively, shear viscosity, bulk viscosity, heat capacity ratio, and thermal conductivity of the gas. The expression clearly shows that dimensionless attenuation monotonically increases with *f/P*.

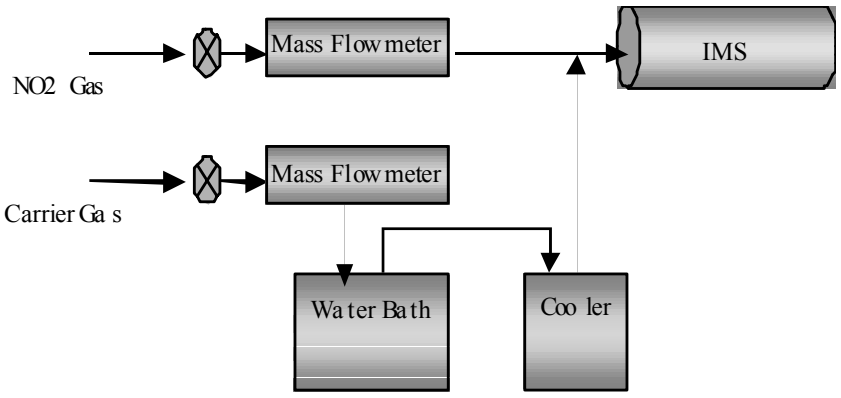

Fig. 2. Schematic diagram of IMS test setup

The classical attenuation in an atomic gas, such as a rare gas represents the total energy absorbed by the gas. But for gases of molecules that contain more than one atom, there are other degrees of freedom that will absorb energy and lead to more attenuation. These degrees of freedom are due to transitions of internal states of the molecules that involve mainly vibrational and rotational

states when acoustic waves propagate in the gas. Typically, molecules will absorb the acoustic energy and return the energy later in the wave cycle. The phenomenon is called acoustic relaxation [8], an irreversible thermodynamic process that transfers energy from the translational mode of motion to the internal modes of the molecule, or to the potential energy of some structural rearrangement. This energy, being absorbed by the gas molecules, reaches its highest value per period when the length of a period equals approximately the time required to achieve equilibrium. Therefore, for differing polyatomic molecules there exist differing acoustic relaxation spectra [9] which may be used to identify gas molecules.

In principle, the acoustic-relaxation problem can be solved by kinetic theory, irreversible thermodynamics, or statistical mechanics. The latter two solutions require rigorous analysis based on collision dynamics and quantum mechanics, which for most cases becomes an insurmountable problem. The irreversible thermodynamics solution has been thoroughly examined [10] and verified by measurements; it generates phenomenological expressions for the speed of sound in irreversible relaxation processes

$$\frac{C^2}{C_o^2} = \frac{1+\omega^2\tau_{PS}^2}{1+(1-\varepsilon)\omega^2\tau_{PS}^2} \tag{7}$$

and attenuation

$$\mu = \frac{\pi\varepsilon}{\sqrt{1-\varepsilon}} \frac{\omega\sqrt{\tau_{PS}\tau_{VS}}}{1+\omega^2\tau_{PS}\tau_{VS}} . \tag{8}$$

In Eqs. 7 and 8, C_o is the isentropic sound speed, μ is the dimensionless attenuation due to relaxation, ε is the relaxation strength, and τ_{PS} and τ_{VS}, respectively, are the adiabatic relaxation times at constant pressure and volume. In general, the relaxation time is inversely proportional to pressure. Hence, attenuation data are normally plotted as μ vs. *f/P*.

From Eq. 8, we can derive the maximum attenuation, given as

$$\mu_{\max} = \frac{\pi\varepsilon}{2\sqrt{1-\varepsilon}} , \tag{9}$$

which occurs at

$$\omega_{\max} = \frac{1}{\sqrt{\tau_{PS}\tau_{VS}}} , \tag{10}$$

or

$$\left(\frac{f}{P}\right)_{\max} = \frac{1}{2\pi\sqrt{1-\varepsilon}\,\tau_{PS}^o} , \tag{11}$$

where τ_{PS}^{o} is the adiabatic relaxation time at constant unit pressure. For ideal gases,

$$\varepsilon = \frac{RC_i}{C_V^o(C_P^o - C_i)}, \tag{12}$$

where C_i is the internal molar heat capacity, which depends on the internal degrees of freedom of the gas molecule. Furthermore, if we assume that the energy transfer between kinetic and internal energy of molecules occurs by means of two-body collisions, the relaxation time can be estimated from the equation

$$\tau_{PS} = \frac{1}{(k + k')N} \frac{(C_P^o - C_i)}{C_P^o}, \tag{13}$$

where k and k' are forward and backward reaction constants that may be estimated from quantum mechanical calculation and N is the gas concentration. For simple diatomic molecules, one may be able to base the estimate of acoustic relaxation spectra on the presented equations. But, for polyatomic molecules, it is easier to measure the spectra than to derive them from the first principle. The relaxation peak for methane was reported at $\approx f/P = 0.2$ MHz/atm [11], which is in a region where the classical attenuation is relatively small so that the total attenuation ($\mu_T = \mu + \mu_{cl}$) will show the characteristic relaxation peak.

4.0 LABORATORY TEST RESULTS AND DISCUSSION

In this section, we present the first-year progress. Tests have been conducted with laboratory prototypes of both sensors. For NO_x sensor development, we have

- Developed a corona/spark discharge ion source,
- Demonstrated the sensor capability to detect both NO and NO_2,
- Evaluated water-vapor effects on IMS and methods to reduce them.

For acoustic-sensor development, we have

- Developed a laboratory prototype,
- Demonstrated the sensor performance with methane gas.

4.1 NO_x Measurement

An ion-mobility spectrometer has been demonstrated as a low-cost gas sensor [12] that can be used in a high-pressure and -temperature environment. Based on ion-molecule chemistry, the basic energy requirement for forming a negative molecular ion is determined by the electron affinity (EA) of the molecule. The EAs for the negative NO and NO_2 ions are ≈0.02 and 2.3 eV, respectively [13]. Therefore, the electron-impact ionization process is likely to produce negative NO and NO_2 ions, but the NO_2 ions are thermodynamically more stable. Furthermore, in a plasma, a neutral NO molecule may be oxidized to form NO_2, especially in the presence of HCs

[14,15]. It is, therefore, possible to estimate the total NO_x emissions by simply measuring NO_2 concentrations.

The feasibility of using ^{63}Ni-IMS to detect negative NO_2 ions has been successfully demonstrated [4]. Because a radioactive source is unacceptable for practical applications, it is desirable to have a nonradioactive ionization source, such as a corona discharge source. Tabrizchi et al. [16] have reported a design of a pulsed corona discharge ionization source that uses a point-to-point geometry. In this work, we describe a pulsed corona discharge ionization source with a needle-to-cylinder geometry; preliminary results of its performance in detecting negative NO_x ions are presented.

4.1.1 IMS Sensor Design

Figure 1 shows the basic design of the IMS sensor. As mentioned earlier, it consists of a pulsed corona discharge ion source, an ion drift tube, and a Faraday plate. The ion source assembly is arranged in a needle/metal-cylinder geometry. During operation, the metal cylinder is biased with a negative voltage so that negative ions will be confined in the cell until the shutter grid opens. The drift tube of the IMS is a glass tube surrounded by a series of steel guard rings that are separated by Teflon rings; this arrangement establishes a uniform electrical field for detecting negative ions. Table 2 lists the specific design parameters and typical operating conditions of the IMS sensor.

Table 2. Design parameters and operating conditions of the IMS sensor

Ion source		Shutter grid			Drift-tube electrical field, V/cm	Detection Electronics		Pressure and Temperature
Needle-surface gap, cm	Applied voltage, kV	Pulse width, ms	Pulse voltage, V	Frequency, Hz		Filter, kHz (LP)[a]	Sensitivity, nA/V	
0.25	-3.0/-4.0	2	140	12.5	220	3	2	ambient

[a]LP = low-pass filter

4.1.2 Laboratory Tests

Laboratory tests were conducted under ambient conditions. Figure 2 shows the IMS experimental setup. Mass flowmeters (MKS 0-500 sccm) were used to provide gas mixtures with known NO_2 concentrations. The water bath and a thermoelectric cooler were incorporated into the carrier-gas line for water vapor tests. Both the sample gas (483 ppm NO_2 in dry nitrogen) and carrier gas (23.6 ppm SO_2, 121.2 ppm H_2, 398 ppm CO, 8.1% O_2, 10% CO_2, and balance N_2) are premixed (provided by AGA Gas, Inc.). Because a typical exhaust gas stream contains ≈10% water, the effect of water on the IMS sensor must be evaluated. The percent water vapor in the carrier gas was controlled by varying the temperature of the water bath. The data acquisition system consists of a low-noise, low-current preamplifier (Stanford Research Systems SR570) and a 16-bit, 100 kS/s digitizer (National Instrument AT-MIO-16E-10).

Typically, 100 averages were used for each ion spectrum that produced a response time of 80 ms. Before quantitative tests were performed, both the flow rate effect and corona discharge characteristics were examined. Figure 3 shows the effect of gas flow rate on the negative-ion spectrum. Slight variations in both amplitude and drift time were measured. The typical flow rate used for the tests was 500 sccm. The discharge ionization source could function in two modes: corona and spark discharge, depending on the applied voltage. The two stages can be easily distinguished from the current measurement, <0.2 mA for corona discharge and >0.5 mA for spark discharge. A 2-MΩ resistor was used in series with the ionization source to stabilize the discharge.

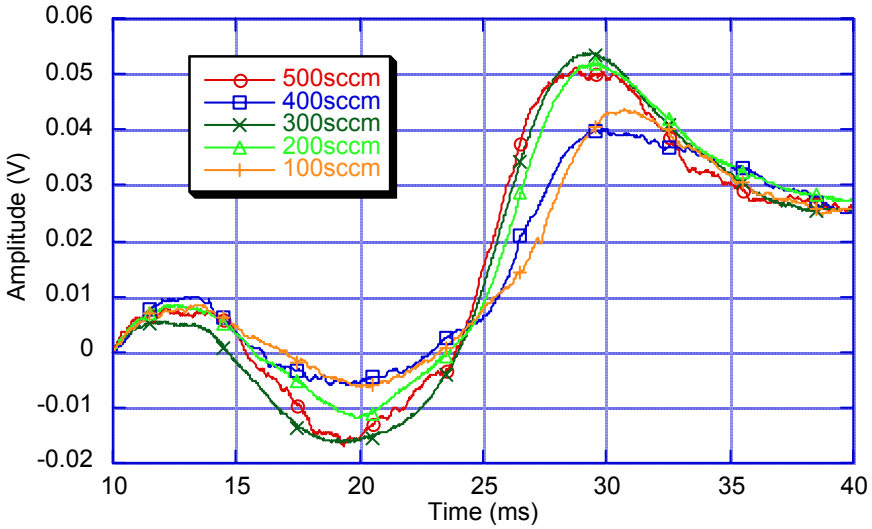

Fig. 3. Negative NO_2 ion spectra at various gas flow rates

4.1.3 Results and Discussion

Figure 4 shows the spectra of a gas mixture with 97 ppm NO_2 in the multicomponent carrier gas obtained under corona and spark discharge modes. The spark discharge (0.8 mA current) produces a peak that is better developed than that obtained in the corona discharge mode (0.1 mA current). A significant difference is noted in drift time between the two spectra. This difference may be due to the in ion-molecule chemistry or the type of ions produced.

Figure 5 shows the corona discharge spectra for four gas mixtures (NO_2/N_2 and carrier gas) with various NO_2 concentrations. The data show that, as NO_2 concentration increases, the ion peak decreases in amplitude but increases in drift time. It was also noticed that the current flowing through the ion source decreased with the peak amplitude, indicating that fewer ions were generated. Furthermore, an ion peak was detected when only carrier gas was introduced, suggesting that, under the corona discharge mode, the primary negative ion produced may be O_2^-, and introduction of NO_2 reduces the O_2^-. A different trend was observed for the spark discharge mode; this is shown in Fig. 6. An increase in peak amplitude was observed with an increase in NO_2 concentration, but the drift time remained relatively unchanged, suggesting that the spark discharge mode of operation may be used to quantify NO_2 concentration by measuring peak amplitude.

The dependence of peak amplitude on NO_2 concentration up to 500 ppm of a NO_2/N_2 gas mixture is shown in Fig. 7. The dependence of amplitude on concentration was also measured, as shown in Fig. 8 for NO_2/carrier-gas mixtures. Quantitatively, the NO_2/carrier-gas mixture produces more ions than the NO_2/N_2 gas mixture. Without introducing NO_2 gas, the carrier-gas mixture shows an ion peak of significant magnitude, with a delay time in the region where the NO_2 ions appear (14.5 – 16 ms). This finding suggests that NO_2 may be produced in the plasma during the spark discharge process if the composition of the buffer gas is the same as the composition of the carrier gas. It is possible that the presence of oxygen (8.1%) in the carrier gas induces the reactions that lead to production of NO_2 ions.

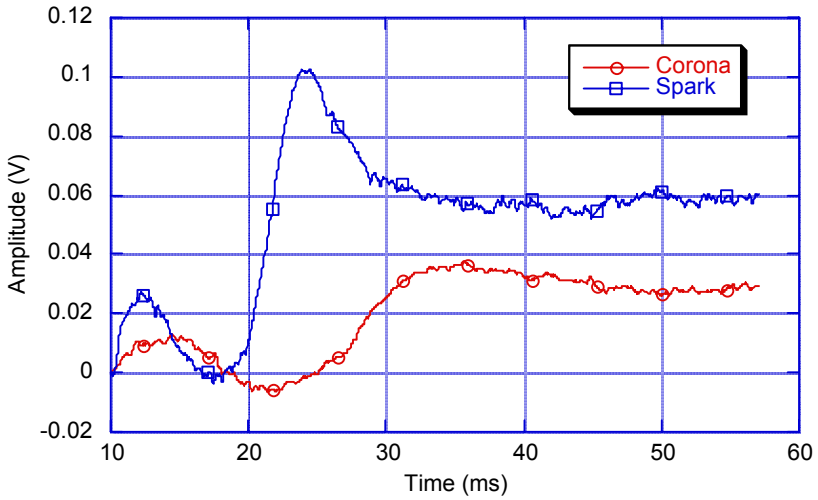

Fig. 4. Spectra of gas mixture with 97% NO_2 in multicomponent carrier gas, produced by corona and spark discharge modes

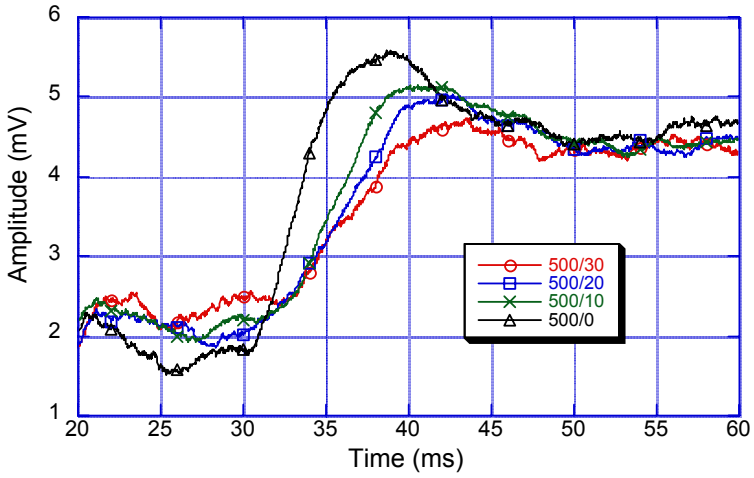

Fig. 5. Negative NO_2 ion peaks produced by corona discharge ionization for four NO_2/N_2 mixtures with constant carrier gas flow (500 sccm) and differing NO_2/N_2 gas flows

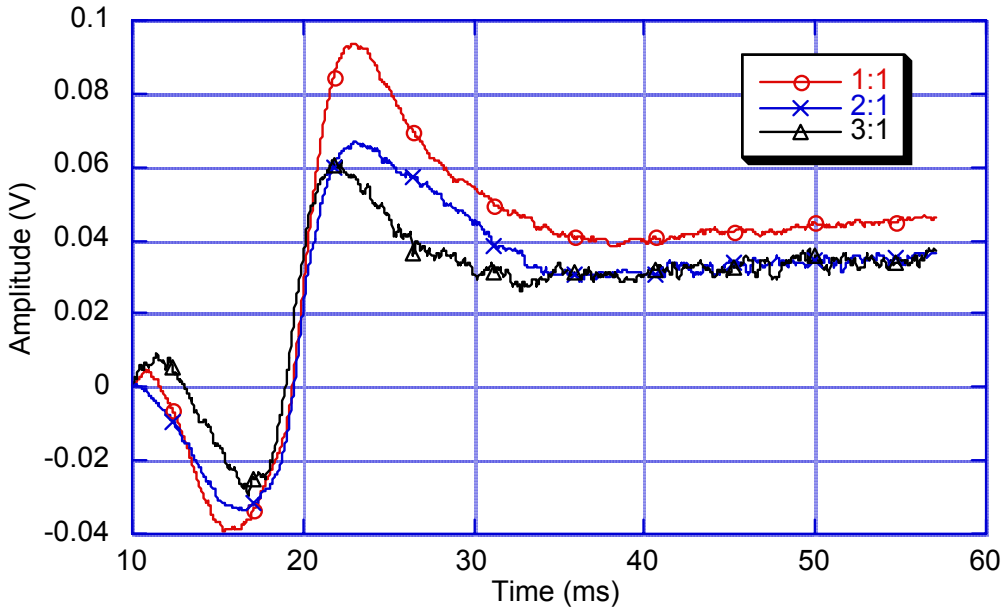

Fig. 6. Negative NO_2 spectra produced by spark discharge ionization of three NO_2/N_2 mixtures, in terms of the carrier/sample gas ratio

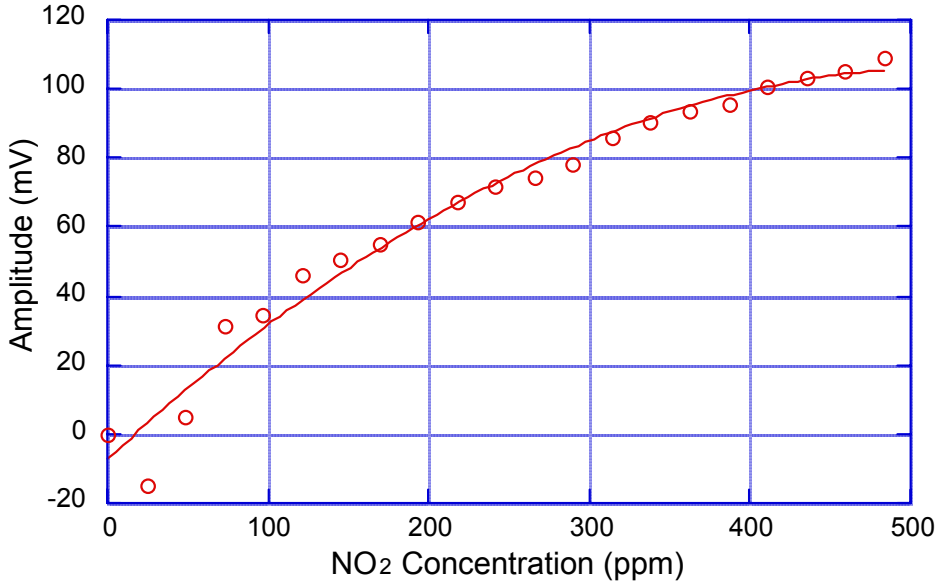

Fig. 7. Peak amplitude vs. NO_2 concentration, measured with dry nitrogen and 2-nA/V sensitivity

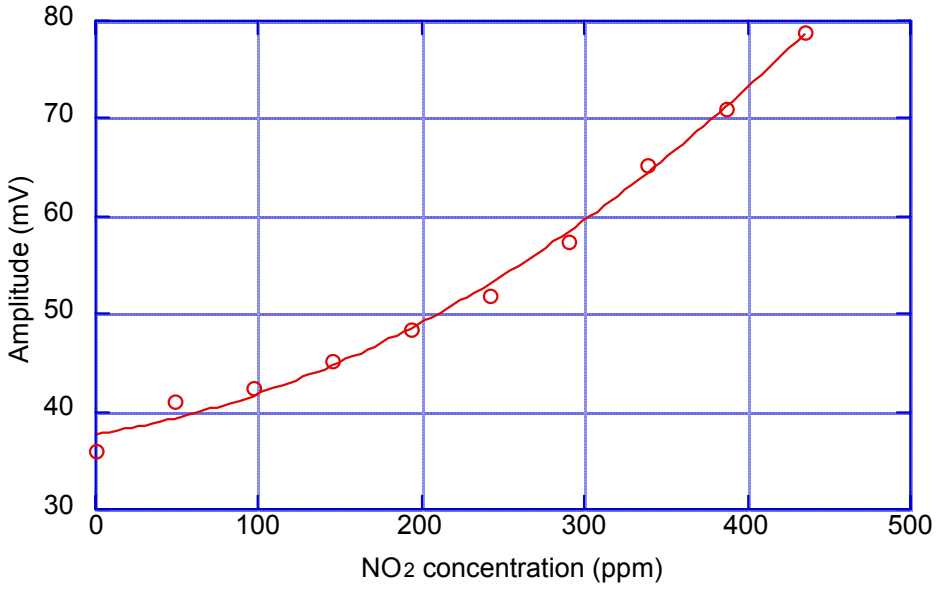

Fig. 8. Peak amplitude vs. NO_2 concentration measured with carrier gas and 5-nA/V sensitivity

The presence of water vapor in IMS tends to degrade the ion spectrum. Figure 9 shows the extent of degradation of the NO_2 ion spectra of gas mixtures that contain various concentrations of water vapor. In most cases, we found that the ion spectrum was completely masked by noise when the vapor content exceeded 1%. Therefore, a method to reduce the noise is necessary for practical applications. We investigated a cooling method that condenses water vapor before the gas enters the IMS.

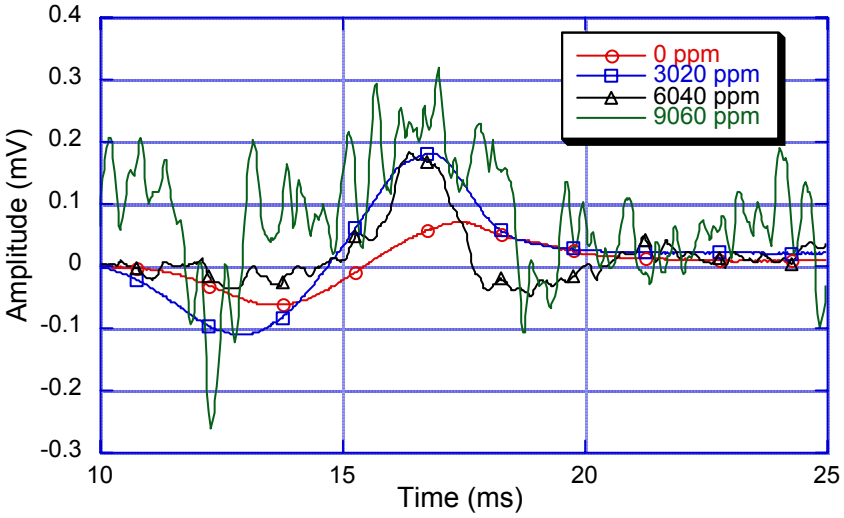

Fig. 9. NO_2 ion spectra of NO_2/carrier-gas mixtures with various water vapor concentrations

Figure 10 shows three ion spectra obtained when vapor-saturated gas passed through a cooling bath that was adjusted to the indicated temperatures. The spectra show that, as temperature decreases, the signal-to-noise ratio improves and the delay time of the peak decreases. The changes in delay time suggest that the size of water clusters may be reduced as the temperature decreases. With the gas flowing through the cold plate before entering the spectrometer, we enable the recovery of the ion spectra. Figure 11 shows the dependence of peak amplitude on concentration when the gas is kept at 0ºC.

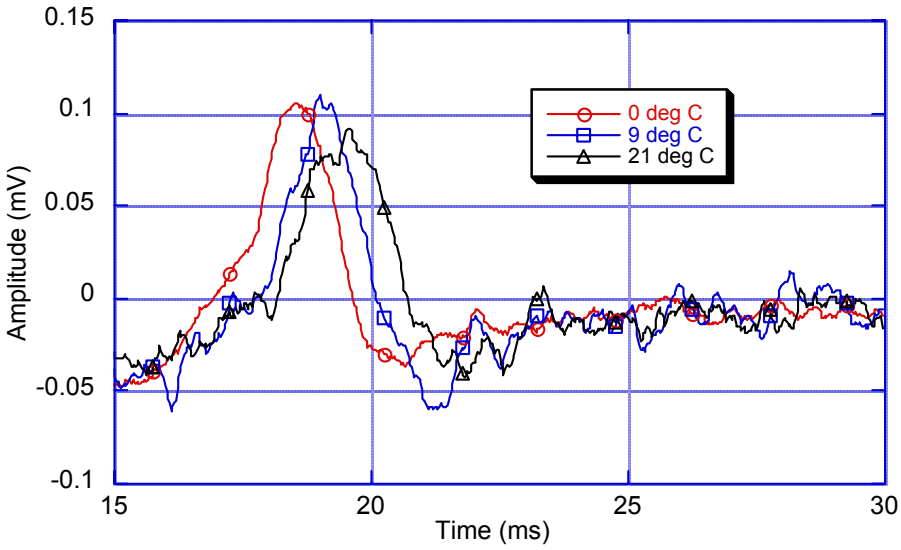

Fig. 10. Negative NO_2 ion peaks detected when carrier-gas temperature is controlled

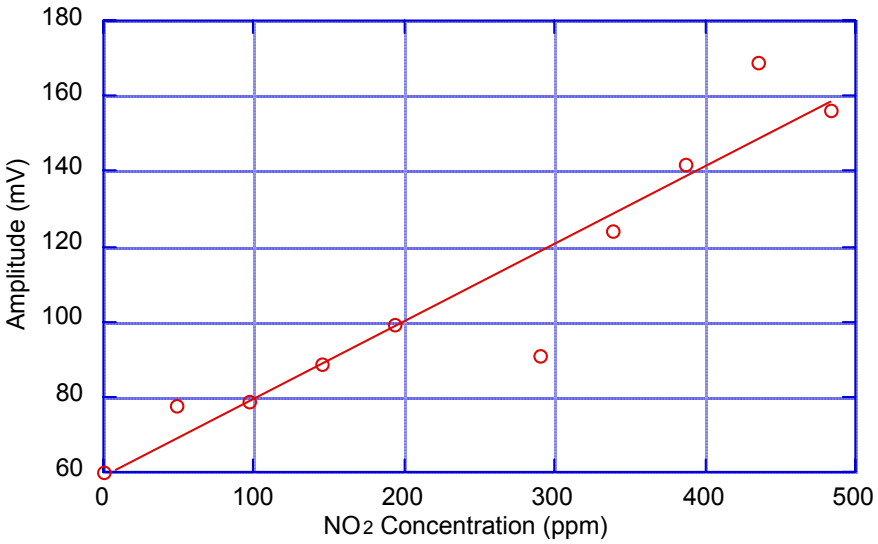

Fig. 11. Amplitude of negative NO_2 ion peak vs. concentration when gas temperature is controlled at 0ºC (2-nA/V sensitivity)

The needle electrode may limit the detection range because of its finite discharge region. To evaluate the effects due to the variation of electrode geometry, we tested a flat-electrode (0.15 x 0.3) design. It was found that the flat electrode requires a voltage >5 kV to produce a spark discharge. When the flat-electrode ionization source was applied to detect nitric oxide (NO) gas in a mixture of nitrogen and NO_x, results were similar to those obtained for NO_2, indicating that current IMS can detect both NO and NO_2 but cannot distinguish the one gas from the other.

A practical NO_2 sensor, based on the IMS technique, is described. The sensor uses a non-radioactive ionization source, operates under ambient conditions, detects negative NO_2 ions, and has a response time of 80 ms. The arrangement of the nonradioactive ionization source is a simple needle-metal-cylinder geometry that allows either corona or spark discharge to develop in the gap between the needle and the cylinder. Preliminary results show that the spark-discharge mode of operation can be used to quantify the NO_2 concentration.

Although we have demonstrated the feasibility of detecting both NO and NO_2 by the IMS technique with a pulsed spark discharge ion source, a few technical hurdles must be overcome before the IMS sensor can be used in a natural-gas engine exhaust environment. These hurdles include (a) effects due to water vapor, (b) drift time ambiguity, and (c) complexity of the ion-molecule chemistry due to variations in exhaust gas composition. To date, the water vapor effect has been examined. Without pretreatment of the gas, the ion spectrum is completely masked by noise when the water content exceeds 1%. Use of a thermoelectric cold plate to condense water from the gas stream before it enters the spectrometer successfully reduced the water effect.

4.2 Natural-Gas Measurement

Figure 12 shows a schematic diagram of the acoustic-sensor laboratory prototype developed at ANL. It consists of two 0.5-MHz transducers that operate in a pitch-catch mode. Gated sine waves of a fixed frequency (0.5 MHz or its harmonics) are propagated in a narrow flow channel, and their reflections are analyzed for variations in amplitude and time-of-flight (TOF), from which attenuation and SOS are measured. The transducers and flow cavity of the prototype are housed in a high-pressure vessel. To obtain the acoustic-relaxation spectra, we vary the gas pressure, because the attenuation in a gas depends on the ratio of acoustic frequency to gas pressure (f/P).

Figure 13 shows the SOS in methane/nitrogen mixtures. Although the measured SOS values are higher than the calculated values, it is clear that the SOS values can be used to predict the methane concentration in nitrogen gas. This is true as long as the composition of the carrier gas mixture is fixed, e.g., air, so that the mixture of methane and carrier gas can be considered a binary gas.

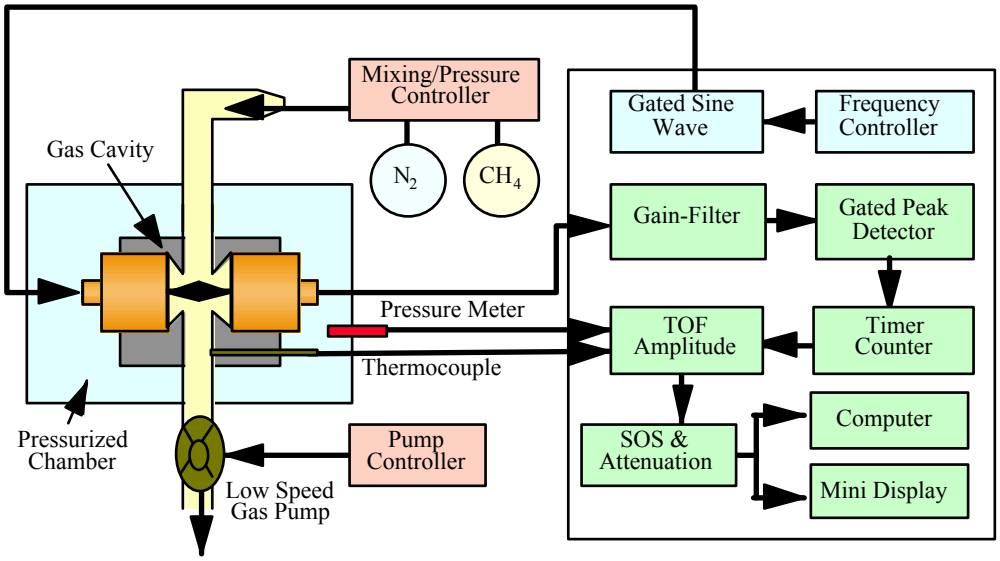

Fig. 12. Diagram of acoustic-sensor laboratory prototype, associated control electronics, and processing system (TOF = time of flight; SOS = speed of sound)

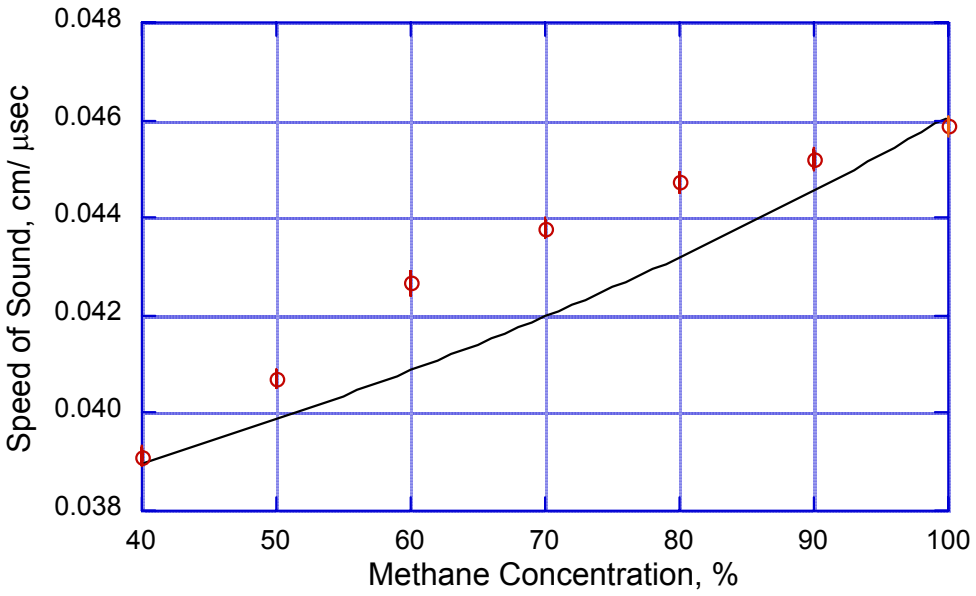

Fig.13. Speed of sound in methane/nitrogen mixtures. Solid line represents calculated values based on isentropic model (Eq. 5).

Figure 14 shows the dimensionless attenuation (attenuation times wavelength, $\alpha\lambda$) for methane/nitrogen mixtures from 40 to 100%. We were somewhat surprised to see that the measured attenuation is less than the classical value. Further research is planned to confirm this

result. In Figure 15, we plot the dimensionless attenuation vs. the frequency/pressure ratio (*f/P*) for 50% methane in nitrogen. It is clear that a relaxation peak exists at x *f/P = 0.07*; under ambient conditions, the relaxation peak appears at 70 kHz. Again, the measured relaxation peak is much lower than the model prediction [3]. Further experiments are planned.

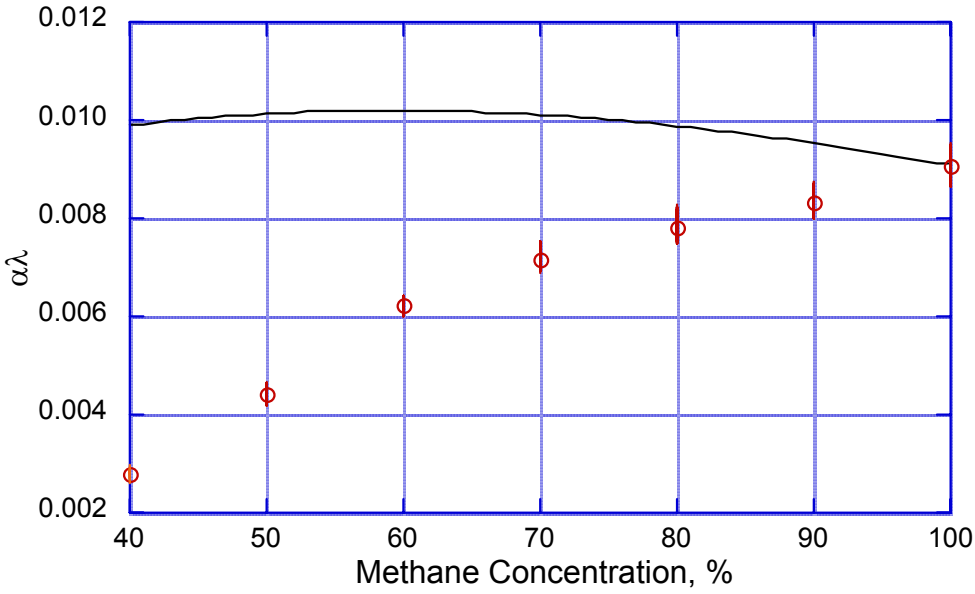

Fig. 14. Dimensionless attenuation for methane/nitrogen mixtures from 40 to 100%. Solid line is calculated classical attenuation (Eq. 6).

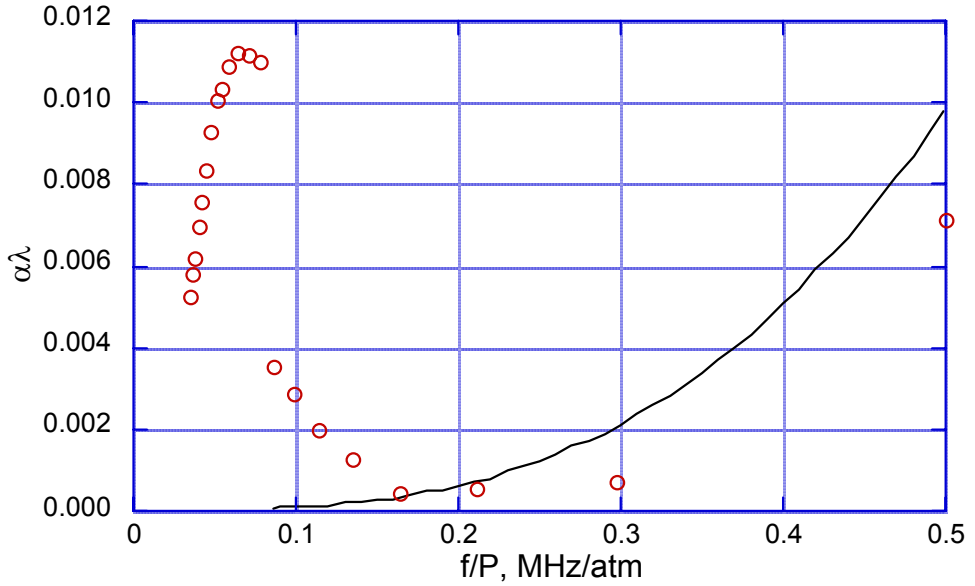

Fig. 15. Dimensionless attenuation vs. f/P for 50% methane in nitrogen. Solid line represents classical attenuation.

In conclusion, in FY 2001, we have demonstrated that (1) the SOS in a fuel-gas/air mixture can be used to measure the percent concentration of the fuel gas, and that (2) it is feasible to use acoustic-relaxation spectra to predict fuel gas composition.

5.0 FUTURE WORK

Further development of the IMS NO_x sensor will focus on the following tasks:

- Determine the sensitivity and reproducibility of the sensor.
- Design and test a prototype field sensor with a cold plate for water removal.
- Develop the control electronics.
- Conduct field tests.

The development of the acoustic natural-gas sensor will consist of the following tasks:

- Establish the acoustic relaxation spectroscopy technique for detecting methane, ethane, and propane.
- Design and test array transducers to measure relaxation.
- Design and test a field sensor to monitor natural-gas concentration.
- Develop an ultrasonic technique to measure gas flow rate.
- Develop the control electronics.
- Conduct field tests.

6.0 REFERENCES

1. E. A. Mason, "Ion mobility: Its role in plasma chromatography," *Plasma chromatography,* Chapter 2, Plenum Press, New York, 1984.
2. M. A. Biondi and L. M. Chanin, "Blanc's law – Ion mobilities in helium-neon mixtures," Phys. Rev. 122, pp. 843-847, 1961.
3. J. A. Jendrzejczyk, S. L. Dieckman, S. Slaughter, and A. C. Raptis, Argonne National Laboratory, personal communication, 1999.
4. J. A. Jendrzejczyk, S. L. Dieckman, S. Slaughter, and A. C. Raptis, Argonne National Laboratory, personal communication, 1999.
5. Data from Advanced Reciprocating Engine System (ARES) consortium, supplied by Gordon R. Gerber of Caterpillar.
6. S. H. Sheen, H. T. Chien, and A. C. Raptis, "Ultrasonic techniques for detecting helium leaks," Sensors and Actuators B 71, pp. 197-202, 2000.
7. *CRC Handbook of tables for applied engineering science*, second edition, CRC Press, Cleveland, OH, 1973.
8. K. F. Herzfeld and T. A. Litovitz, *Absorption and dispersion of ultrasonic waves,* Academic Press, New York, 1959.
9. H. J. Bauer, "Phenomenological theory of the relaxation phenomena in gases," in *Physical acoustics,* Vol. II Part A, Academic Press, New York, pp. 48-132, 1965.
10. H. O. Kneser, "Phenomenological theory of the relaxation phenomena in gases," in *Physical acoustics,* Vol. II Part A, Academic Press, New York, pp. 133-202, 1965.
11. D. Sette, A. Busala, and J. C. Hubbard, "Energy transfer by collisions in vapors of chlorinated methanes," J. Chem. Phys. 23, pp. 787-793, 1955.
12. G. A. Eiceman and Z. Karpas, *Ion mobility spectrometry*, CRC Press, Ann Arbor, MI, 1994.
13. B. M. Smirnov, *Negative ions*, McGraw-Hill Inc., New York, pp. 27-31, 1982.
14. B. M. Penetrante, W. J. Pitz, M. C. Hsiao, B. T. Merritt, and G. E. Vogtlin, "Effect of hydrocarbons on plasma treatment of NO_x," Proceedings of the 1997 Diesel Engine Emissions Research Workshop, San Diego, CA, July 28-31, 1997, pp. 123-128.
15. S. G. Ejakov, H.-T. Chien, R. Dorai, J. A. Jendrzejczyk, A. C. Raptis, S.-H. Sheen, and J. H. Visser, "Modeling the use of a plasma source in ion-mobility spectrometry for NO_x detection in automotive exhaust," Proc. of 2001 Int'l Symp. of Ion Mobility Spectrometry.
16. M. Tabrizchi, T. Khayamian, and N. Taj, "Design and operation of a corona discharge ionization source for ion-mobility spectrometry," Rev. Sci. Inst. 71(6), pp. 2321-2328, 2000.

Distribution for ANL-01/29

Internal

J. L. Carlson (2)
H.-T. Chien (10)
H. Drucker
N. Gopalsami
J. A. Jendrzejczyk
L. Johnson
J. Harmon
R. B. Poeppel
A. C. Raptis
W. Schertz
S.-H. Sheen (15)
R. A. Valentin
TIS Files

External

U.S. Department of Energy
Office of Power Technology
J. A. Mavec
J. M. Livengood
Caterpillar, Inc.
G. Gerber
Cummins Engine Company, Inc.
D. A. Bolis
Waukesha Dresser
R. J. Kakoczki
Energy Technology Division Review Committee
H. K. Birnbaum, University of Illinois at Urbana-Champaign
I.-W. Chen, University of Pennsylvania
F. P. Ford, Rexford, NY
S. L. Rhode, University of Nebraska - Lincoln
H. S. Rosenbaum, Fremont, CA
S. L. Sass, Cornell University
R. Zoughi, University of Missouri-Rolla